

Published in IET Control Theory and Applications
 Received on 26th July 2009
 Revised on 31st December 2009
 doi: 10.1049/iet-cta.2009.0377



H_∞ design of rotor flux-oriented current-controlled induction motor drives: speed control, noise attenuation and stability robustness

J.C. Basilio J.A. Silva Jr L.G.B. Rolim M.V. Moreira

*Universidade Federal do Rio de Janeiro, COPPE - Programa de Engenharia Elétrica, Cidade Universitária, Ilha do Fundão, 21.949-900, Rio de Janeiro, R. J., Brazil
 E-mail: basilio@dee.ufrj.br*

Abstract: This study deals with the design of H_∞ controllers for speed control of rotor flux-oriented current-controlled induction motors. The mixed sensitivity problem (robust stability and performance) is initially revisited, and is shown, based on practical experiments, that when the rotor time constant is the uncertain parameter, it is necessary to deploy conflicting weighting functions, therefore invalidating its application in the design of current-fed induction motors. Two other H_∞ problems are addressed: (i) a one-block problem for speed control with tracking and transient performance objectives; and (ii) a two-block problem for speed control with tracking/transient performance and noise attenuation objectives. An important part of H_∞ design is the model of the system to be controlled. In this study, the system composed of the inverter, estimator and induction motor will be modelled as a first-order system, and experiments for the identification of the gain and the time constant are proposed. It is also suggested how to properly correct an initial estimation of the rotor time constant in order to make the actual plant (inverter-induction motor) behave as a first-order linear system. The model accuracy and the efficiency of the H_∞ controllers are validated by experiments carried out in a real system.

1 Introduction

Although induction motors are mathematically described by non-linear models, the use of Blaschke transformation [1] leads to an equivalent linear model, the so-called field-oriented or vector-controlled induction motors, which can be voltage- or current controlled. The main advantage of using field-oriented control of voltage-controlled induction motors is that performance can be improved with exact input-output decoupling and linearisation, and can be achieved via non-linear state feedback [2]. On the other hand, field-oriented control of current-controlled induction motors has a first-order model whose input and output are, respectively, the quadrature component of the stator current and the angular velocity [3].

Although appealing from the theoretical point of view, controller design for either voltage- or current-fed vector-controlled induction motors requires exact knowledge of the rotor resistance and some information on flux. The former requires the measurements of the a - b flux components, which requires the introduction of flux sensing coils or Hall effect transducers in the stator – therefore being not realistic in general-purpose squirrel cage machines – whereas the latter requires the knowledge of the rotor flux angle. These limitations provide an ideal scenario for the design of H_∞ controllers [4] to both current- and voltage-controlled induction motors. Although H_∞ controller theory has been criticised on account of controller fragility [5], a recent paper has proved it wrong [6], that is H_∞ controllers are also reliable as far as fragility is concerned.

The application of H_∞ control theory to current-fed vector-controlled induction motor drives has received a great deal of attention in the literature. The first application appears in [7], where the so-called mixed sensitivity problem

$$\min_{K(s) \text{ stabilising}} \left\| \begin{bmatrix} W_S S \\ W_T T \end{bmatrix} \right\|_\infty \quad (1)$$

is considered. In (1), $S(s) = [I + G(s)K(s)]^{-1}$ denotes the sensitivity function and $T(s) = 1 - S(s) = G(s)K(s)S(s)$ represents the closed-loop transfer function, with $G(s)$ and $K(s)$ respectively, being, the plant and controller transfer functions. The weights $W_S(s)$ and $W_T(s)$ were chosen in [7] based on the assumption that $W_S^{-1}(s)$ and $W_T^{-1}(s)$ serve as upper bounds for $S(s)$ and $T(s)$, respectively. Although the designed controllers were tested in an experimental set-up, no practical consideration has motivated the choice of $W_T(s)$; indeed no practical issues such as the lack of exact knowledge of the rotor time constant were taken into account in the choice of $W_T(s)$. In a subsequent work [8], H_∞ control theory was applied to design a state feedback static controller for speed control. The solution to the problem proposed in [8] has been obtained using the Doyle–Glover–Khargonekar–Francis (DGKF) approach [9], which means that another control objective, besides speed control, has been addressed; however, neither the H_∞ problem that has been considered nor any consideration on the definition of weights and their choices have been explicitly given in [8]. More recently, using the degrees of freedom available in the Youla–Kucera parametrisation for all two-degree-of-freedom stabilising controllers. Gan and Qiu [10] propose the design of a plug-in (additional) H_∞ compensator to improve the robustness of the closed-loop system against the change in the rotor resistance. The use of the two-degree-of-freedom structure has been supported only by mathematical reasons, namely that the choice of the stable proper rational free parameter of the Youla–Kucera parametrisation does not affect the transfer function that relates the reference signal and the output to be controlled. In none of the works cited above, the problems of reducing the effect of measurement noise in the control signal and the systematic choice of weights $W_S(s)$ and $W_T(s)$ for flux-oriented current-controlled induction motors have been addressed.

The design of H_∞ controllers for feedback-linearised induction motor has been considered in [11–15]. A robust speed control strategy has been proposed in [11]. An H_∞ disturbance attenuation approach has been presented in [12]. H_∞ controllers for the mixed sensitivity problem (1) have also been obtained in [13, 14]. In [15], the design of an H_∞ robust controller for the automatic positioning of a mechanical load connected to an induction motor via a flexible joint is considered. H_∞ control theory has also been applied to the design of a full-order observer for vector-controlled induction motors using gain-scheduled H_∞ control and linear matrix inequality (LMI) [16].

The main objective of this paper is to bridge the gap between theory and practice observed in [7, 8, 10]. The

mixed sensitivity problem (1) is initially addressed and is explained how weight $W_T(s)$ is obtained in practice to account for the non-exact knowledge of the rotor time constant. It is concluded, based on practical experiments, that using the usual one-degree-of-freedom controller structure, the mixed sensitivity problem cannot address simultaneously the objectives of performance and robustness with respect to uncertainty in the estimated value of the rotor time constant. In the sequel, assuming that the angular speed is the variable to be controlled and measured, two other control objectives are considered: (i) closed-loop system performance and (ii) attenuation of the effects of noise measurement on the control signal (input current to the induction motor). Problem (i) is addressed by means of a one-block H_∞ problem and problem (ii) is formulated as a two-block H_∞ problem. Their solutions are synthesised in two design procedures, allowing easy application of the theoretical results developed in the paper by engineer practitioners.

An important part of H_∞ controller design is the model of the system to be controlled. In this paper, the system composed of the inverter, estimator and induction motor will be modelled as a first-order system, and experiments for the identification of the gain and the time constant are proposed. It is also suggested how to properly correct an initial estimation of the rotor time-constant in order to make the actual plant (inverter-induction motor) behave as a linear first-order system. The model accuracy and the efficiency of the H_∞ design strategy are validated by experiments carried out in a real system.

The paper is structured as follows. Section 2 presents a brief theoretical background on rotor flux-oriented current-fed induction motors, proposes an experimental procedure for the identification of the model parameters, and applies the proposed procedure to the identification of the parameters of a real induction motor. Section 3 approaches three H_∞ problems: (i) the mixed sensitivity problem formulated according to (1) (from a practical point of view); (ii) a one-block H_∞ problem for speed control with tracking and transient performance objectives and (iii) a two-block H_∞ problem for speed control with tracking/transient performance and noise attenuation objectives. Section 4 presents experimental results to validate the design strategies proposed in the paper. Finally, conclusions are drawn in Section 5.

2 Linear model for rotor flux-oriented control of current-fed induction motors

2.1 Mathematical model

Assuming as inputs, the stator current vector components in field coordinates, $i_{s_d}(t)$ (the stator current component in the direction of the magnetising current vector, usually referred to as the direct component), and $i_{s_q}(t)$ (the quadrature

component of the stator current, which is perpendicular to $i_{sd}(t)$, then current-fed induction motors can be modelled as [3]

$$T_R \frac{d}{dt} i_{mR}(t) + i_{mR}(t) = i_{sd}(t) \quad (2)$$

$$\frac{d}{dt} \rho(t) = \omega(t) + \frac{i_{sq}(t)}{T_R i_{mR}(t)} \quad (3)$$

and

$$J \frac{d}{dt} \omega(t) + f \omega(t) = k i_{mR}(t) i_{sq}(t) \quad (4)$$

where $T_R = L_R/R_R$ denotes the rotor time constant, L_R and R_R are, respectively, the rotor inductance and resistance, $i_{mR}(t)$ is the magnetising current, $\rho(t)$ is the rotor flux angle with respect to the stator axis, J is the motor inertia, f is the viscous friction, $\omega(t)$ is the instantaneous angular velocity of the rotor and k is the coupling factor, which is a function of the total leakage factor of the motor and of the stator inductance. Note that, if in (2), the direct component of the stator current is made constant, that is, $i_{sd}(t) = I_{sd}$, then, after a brief transient, dictated by the rotor time constant T_R , $i_{mR}(t)$ becomes equal to I_{sd} . When this happens, the electrical torque becomes a function of $i_{sq}(t)$ only, and thus, the model of a current-fed induction motor becomes analogous to that of a constant field dc-motor controlled by the armature current. However, $i_{sq}(t)$ and $i_{sd}(t)$, are not accessible, being functions of the line currents $i_{s1}(t)$, $i_{s2}(t)$ and $i_{s3}(t)$, as follows

$$\begin{bmatrix} i_{sd}(t) \\ i_{sq}(t) \end{bmatrix} = T \begin{bmatrix} i_{s1}(t) \\ i_{s2}(t) \\ i_{s3}(t) \end{bmatrix} \quad (5)$$

where

$$T = \begin{bmatrix} \frac{3}{2} \cos \rho(t) & \frac{\sqrt{3}}{2} \sin \rho(t) & -\frac{\sqrt{3}}{2} \sin \rho(t) \\ -\frac{3}{2} \sin \rho(t) & \frac{\sqrt{3}}{2} \cos \rho(t) & -\frac{\sqrt{3}}{2} \cos \rho(t) \end{bmatrix}$$

The alternating currents $i_{s1}(t)$, $i_{s2}(t)$ and $i_{s3}(t)$ are obtained by applying to $i_{sd}(t)$ and $i_{sq}(t)$ the inverse transformation $T^\dagger = T^T(TT^T)^{-1}$, where $(\cdot)^T$ denotes matrix transposition. This is done in practice with current-controlled inverters [17, 18] (here simply referred to as inverter). The inverter inputs are the desired values for the direct and quadrature components of the stator current, here denoted as $i_{sd,ref}(t)$ and $i_{sq,ref}(t)$ and, its outputs are the line currents $i_{s1}(t)$, $i_{s2}(t)$ and $i_{s3}(t)$ necessary to make $i_{sd}(t)$ and $i_{sq}(t)$ (the actual values) equal to their reference values.

Assuming that $i_{sd,ref}(t) = I_{sd,ref}$ (constant), then the transfer function for the system that consists of an ideal inverter and a current-fed induction motor relating $i_{sq,ref}(t)$ and $\omega(t)$ is given by

$$G(s) = \frac{\Omega(s)}{I_{sq,ref}(s)} = \frac{k I_{sd,ref}}{J s + f} = \frac{k_{abs} I_{sd,ref}}{\tau s + 1} \quad (6)$$

where $\tau = J/f$ and $k_{abs} = k/f$.

Although appealing from the theoretical point of view, this approach has the following drawback: since the rotor flux angle $\rho(t)$ cannot be measured, it has to be estimated. However, as shown in Fig. 1, its estimate ($\hat{\rho}(t)$) depends on the knowledge of the rotor time constant T_R , whose value cannot be determined precisely. If the estimated value

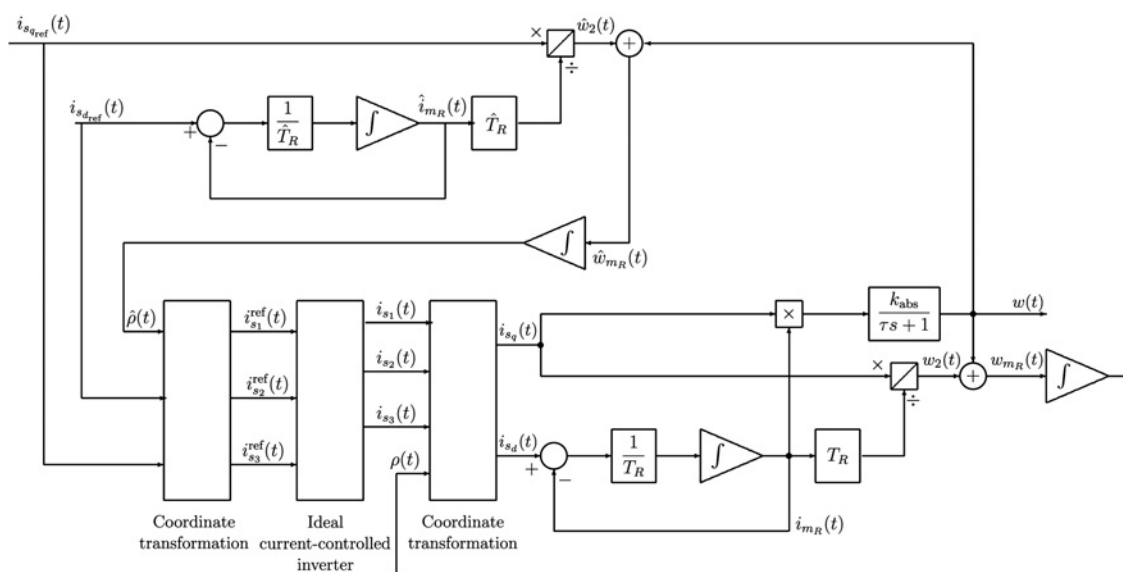


Figure 1 Block diagram of an ideal inverter in cascade with a current-fed induction motor, and with a rotor flux angle estimator

of the rotor time constant (here denoted as \hat{T}_R) is exactly equal to T_R , then the behaviour of the system that consists of the estimator, inverter and induction motor is the same as that described by (6). However, in general $\hat{T}_R \neq T_R$, and thus (6) is no longer a reliable model for the system. Therefore the idea of taking into account the uncertainty of T_R in the design of speed controller for induction motors arises naturally. One of the most appropriate design techniques to deal with model uncertainty is the H_∞ control theory. It is well known that H_∞ controller design relies on a mathematical model of the system. Therefore before addressing the design problem, experiments to obtain nominal values for parameters k_{abs} and τ of (6) will be proposed.

2.2 Parameter identification

According to the model given in (6), the parameters to be determined are k_{abs} , $I_{s_{\text{dref}}}$ and τ . In addition, as shown in Fig. 1, it is also necessary to estimate T_R . These parameters can be estimated as follows:

1. The value of $I_{s_{\text{dref}}}$ can be obtained experimentally by varying slowly $I_{s_{\text{dref}}}$ from 0A until the motor starts to rotating.

2. An estimation of T_R can be found in two steps: first, an initial estimation of T_R (here denoted as \hat{T}_{R_0}) is obtained; second, small corrections in this initial estimation are made in order to obtain a new estimation \hat{T}_R that is closer (than \hat{T}_{R_0}) to the actual value of T_R . The initial estimation \hat{T}_{R_0} can be obtained by either performing standard tests for determining the parameters of the steady-state circuit model [19], or by using online estimation techniques (see [20] and the references therein). The correction in \hat{T}_{R_0} is justified by the fact that the system that consists of the inverter, estimator and induction motor behaves as an ideal first-order system only when the estimated value of the rotor time constant is exactly equal to its actual value. Therefore as the model given in (6) is that of a first-order system, \hat{T}_{R_0} needs correction whenever the system step response differs from that of a first-order system. This suggests the following experiment for the identification of k_{abs} and τ and to find an estimated value \hat{T}_R closer (than \hat{T}_{R_0}) to T_R .

Experiment procedure 1

Step 1: Apply a step input $i_{s_{\text{dref}}}(t) = I_{s_{\text{dref}}}$, $t \geq 0$, to the induction motor and record the output $w(t)$. Let $(t_i, w(t_i))$, $i = 1, \dots, N$ denote all the ordered pairs for the recorded $w(t)$.

Step 2: Using the points $(t_i, w(t_i))$, $i = 1, \dots, N$ obtained in step 1, find a first order model (using any identification method).

Step 3: Apply the same step input of step 1 to the model obtained in step 2, and record the output $(t_i, \hat{w}(t_i))$; this can be easily done using Matlab/Simulink.

Step 4: Compute $E = \int_0^\infty e^2(t) dt$, the square of the ℓ_2 norm of the error $e(t) = w(t) - \hat{w}(t)$, using the points obtained in steps 2 and 3; a good approximation for E can be calculated using the Matlab function 'trapz'.

Step 5: Define a threshold value E_{max} for E . If $E > E_{\text{max}}$ then, increase or decrease T_R , appropriately, and repeat steps 1 to 4, for the current value of $I_{s_{\text{dref}}}$. If $E \leq E_{\text{max}}$, make the values of $k_{\text{abs}}I_{s_{\text{dref}}}$ and τ , defined in (6) equal to the gain and the time constant of the model obtained in step 4, and adopt the current value of T_R as the estimation for the rotor time constant \hat{T}_R , and go to step 6.

Step 6: If there are larger values of $I_{s_{\text{dref}}}$ inside the desired operation region of the induction motor, choose a larger value for $I_{s_{\text{dref}}}$, and go back to step 1. Otherwise, stop.

Remark 1: How close the value of \hat{T}_{R_0} is to the real value of T_R determines the number of iterations needed in step 5 of experimental procedure 1. It is worth noting that once the induction motor step response is close (up to a threshold value) to the step response of an ideal first order system, there is no need for additional changes in the value of \hat{T}_R . \square

2.3 Model validation

A 30 V, 4.6 A, 130 W, 60 Hz, two-pole, delta-connected, squirrel-cage induction motor with $J = 0.00057 \text{ kg m}^2$ has been used for experimentation. All the control tasks are implemented using Simulink real-time windows target running under Windows XP on a Pentium IV, 2.6 GHz. The sampling frequency is set to 5 kHz. The motor currents are measured with Hall-effect transducers (LEM LA-55P, with 0.65% of accuracy) and read by the control program through a 12 bit A/D converter on a dedicated interface board (Advantech PCI-1711). Current control is performed by a synchronous on-off algorithm [3] that operates independently for each leg of a three-phase insulated gate bipolar transistor (IGBT) inverter bridge. Each IGBT in the inverter bridge is driven by a separate digital signal, which is directly issued by the control program at each sampling period, through digital output ports on the interface board. Dead times are properly inserted by an external circuit, to prevent leg shoot-through. An incremental encoder with 10 bit resolution is used for the measurement of rotor angular speed. An electronic circuit having a frequency-voltage converter based on IC 2917 plus a logic that sets the algebraic sign according to the rotation direction provides the interface between the encoder and the analogue input of the board.

Following the directions for the determination of $I_{s_{\text{dref}}}$, it has been obtained $I_{s_{\text{dref}}} = 2.65 \text{ A}$, which will be used in all experiments reported in the paper.

An initial estimate $\hat{T}_{R_0} = 0.0519 \text{ s}$ has been obtained by performing the experiments proposed in [19]; however, as

pointed out before, any online method for the estimation of T_R could be deployed. Following experimental procedure 1, it has been found that $\hat{T}_R = 0.0493$ s, which is approximately 5% smaller than \hat{T}_{R_0} .

Table 1 presents the gains and the time constants for the first-order model obtained by applying step signals in $i_{sdref}(t)$ with the amplitudes shown in the first column; it is worth remarking that a step of amplitude 0.5 A was initially applied to $i_{sdref}(t)$ to avoid the dead zone. Average values for k_{abs} and τ have been adopted using the data of Table 1, being given as $k_{abs} = 108.6936$ A rad/s and $\tau = 4.8703$ s. Fig. 2 shows the comparisons between results obtained experimentally (solid lines) and from simulation (dashed lines) by applying step signals of amplitudes 0.2 (top plot) and 1.0 (bottom plot) to the real system and to a Simulink model equivalent to the block diagram of Fig. 1 (with the estimated values of k_{abs} , τ and $T_R = \hat{T}_R$). It is worth remarking that the Simulink model used in the validation process is not the same as that described at the beginning of

this section. Note that there is only a small difference between simulated and real response during transient and that the steady-state response of the model cannot be distinguished from that of the real system, which attests the accuracy of the estimation of τ and k_{abs} . Therefore it can be concluded that the experimental procedure proposed in this section has actually led to an accurate first-order model for the system that consists of the inverter, estimator and induction motor.

3 H_∞ design of rotor flux-oriented controlled induction motor drives

3.1 Problem formulation

The block diagram for the control problem addressed in this paper is depicted in Fig. 3, where $\Omega_r(s)$, $\Omega(s)$, $E(s)$, $\mathcal{N}(s)$ and $I_{sdref}(s)$ denote, respectively, the Laplace transforms of the reference and actual speed signals, the error signal, the measurement noise and the reference signal for the direct component of the stator current, here assumed as the control variable, $G(s)$ denotes the transfer function of the system to be controlled (inverter–estimator–induction motor) and $K(s)$ is the controller transfer function to be designed. It is assumed, for design purposes, that there is no delay in the inversion–estimation stage.

The problems to be considered in this paper are as follows:

P1. Performance and robust stability against uncertainty in the knowledge of the rotor time constant T_R ;

Table 1 Values of k_{abs} and τ calculated for each step response experiment

Step amplitude	k_{abs} , rad/s/A	τ , s
0.2	111.3399	4.4073
0.4	103.1776	4.8545
0.6	107.2638	5.1912
0.8	110.5254	4.8258
1.0	111.1809	5.0728

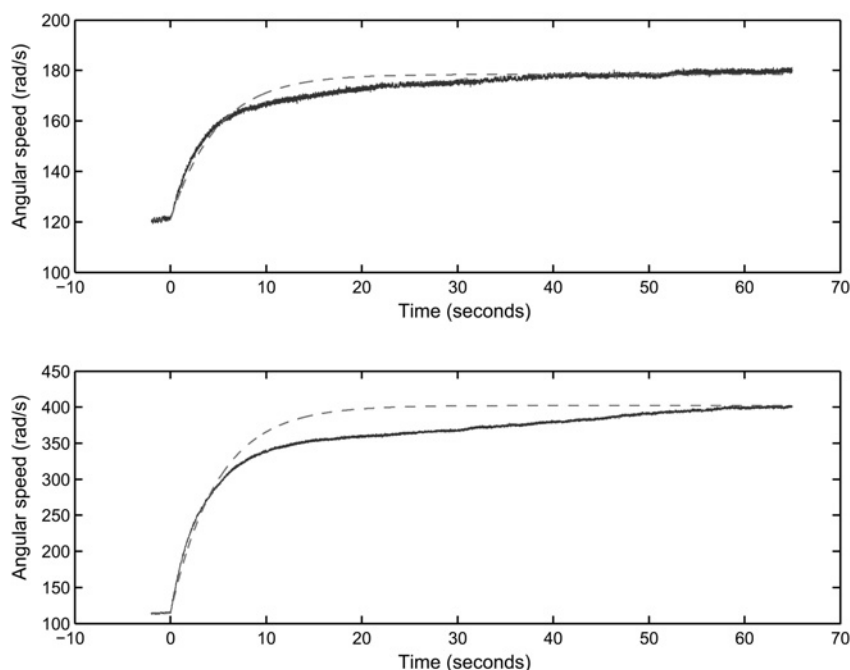


Figure 2 Step responses for the real system (dashed lines) and for the Simulink model (dashed lines) for steps of amplitudes 0.2 A (top plot) and 1.0 A (bottom plot)

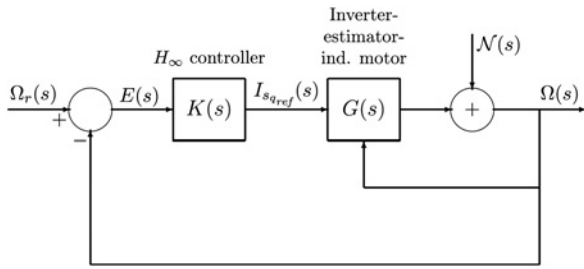


Figure 3 Block diagram for the design of H_∞ speed controllers of rotor flux-oriented controlled induction motor drives

P2. Speed control with tracking and transient performance objectives;

P3. Speed control with tracking, transient performance and attenuation of the effects of measurement noise $\eta(t)$ in the control signal $i_{s_{dref}}(t)$.

These problems will be addressed using H_∞ control theory. The corresponding formulations and solutions are presented in the sequel.

3.2 Two-block H_∞ problem for performance and robust stability against uncertainty in the knowledge of T_R

Tracking/transient performance and robust stability objectives are addressed simultaneously by solving the following H_∞ optimisation problem

$$\text{Prob. P1 } \min_{K(s) \in \mathcal{S}} \left\| \begin{bmatrix} W_S S \\ W_T T \end{bmatrix} \right\|_\infty \quad (7)$$

where \mathcal{S} is the set of all stabilising controllers, $W_S(s)$ is a weighting function used to penalise the relevant frequencies of the signal to be tracked and $W_T(s)$ is obtained from practical experiments and gives a quantitative measure on how model parameter uncertainty affects the nominal model of the system. Note that, as $T(s) + S(s) = 1$, the control objectives addressed in (7) are conflicting, and therefore in order to consider both objectives simultaneously, the weighting functions $W_T(s)$ and $W_S(s)$ must penalise different frequencies; for example, in linear systems, frequency response identification usually leads to more imprecise description at high frequencies, and thus, in this case, $W_T(s)$ must be a high-pass transfer function. On the other hand, signals to be tracked have usually a pre-defined low frequency, and thus, $W_S(s)$ must be a low-pass transfer function.

In a rotor flux-oriented current-controlled induction motor, the main cause for parameter uncertainty is the inexact knowledge of the rotor time constant. Therefore $W_T(s)$ should be determined to account for the variation of the rotor time constant. In order to do so, it is worth noting that the mixed sensitivity problem given

in (7) is formulated assuming unstructured multiplicative uncertainty in $G(s)$, that is

$$G_p(s) = [1 + W_T(s)]G(s) \quad (8)$$

where $G(s)$ is obtained for the nominal value of \hat{T}_R and $G_p(s)$ accounts for perturbations on \hat{T}_R . It is clear from (8) that, for each frequency ω_k , the following relationship holds true

$$\frac{G_p(j\omega_k)}{G(j\omega_k)} - 1 = W_T(j\omega_k) \quad (9)$$

Thus, it is straightforward to see that

$$\left| \frac{G_p(j\omega_k)}{G(j\omega_k)} - 1 \right| \leq |W_T(j\omega_k)| \leq \left| \frac{G_p(j\omega_k)}{G(j\omega_k)} + 1 \right| \quad (10)$$

Fig. 4 shows the results obtained experimentally by applying $i_{s_{dref}}(t) = I_{s_{dref}}^o + I_{s_{dref}}^{\max} \sin(\omega_k t)$ to the real set-up described in Section 2.3, and computing the gains at each frequency ω_k for $I_{s_{dref}}^o = 0.6$ A, $I_{s_{dref}}^{\max} = 0.3$ A, and ω_k equal to 1.4, 2.2, 3.3, 5.0, 7.7, 11.6, 17.9, 27.6, 41.0 and 63.2 rad/s, for \hat{T}_R (ball-dotted line), for a perturbation of +50% in \hat{T}_R (cross-dotted line) and for a perturbation of -50% in \hat{T}_R (star-dotted line). A first-order weighting function, defined according to (8) can then be obtained by adjusting the points obtained experimentally. For the points shown in Fig. 4

$$W_T(s) = \frac{0.2(s + 131)}{s + 23} \quad (11)$$

has been obtained. Note that this weighting function satisfies (10) for each ω_k , as shown in Fig. 4 (solid lines).

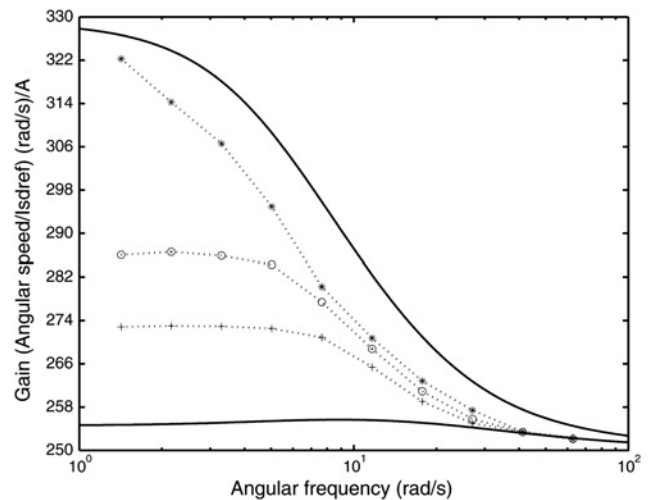


Figure 4 Experimental results obtained for $\hat{T}_R = 0.0493$ s ($\cdot \circ \cdot$) and by perturbing \hat{T}_R in +50% ($\cdot + \cdot$) and -50% ($\cdot * \cdot$) and $|G(j\omega)| |1 \pm W_T(j\omega)|$ (solid lines)

Before solving H_∞ problem P1, it is worth analysing the weighting functions $W_S(s)$ and $W_T(s)$. As steps are usually the class of signals to be tracked in practice, $W_S(s)$ must be a low-pass rational function. Consequently, $|S(j\omega)|$ will be small at low frequencies. On the other hand, as $S(s) + T(s) = 1$, then $|T(j\omega)|$ will be large at low frequencies, therefore $W_T(s)$ should not penalise low frequencies. As pointed out before, this difficulty is easily overcome in linear systems, because parameter uncertainty in linear systems is mainly due to neglected dynamics, which are characterised by high-frequency poles. However, the rational function given by (11) places more penalty at low rather than at high frequencies, and thus, the usual H_∞ control theory assumption that $W_T(s)$ is a high-pass transfer function does not apply to rotor flux-oriented current-controlled induction motor drives, since $W_T(s)$ obtained experimentally is a low-pass transfer function. As a consequence, the two-block H_∞ problem given in (7) cannot be used to address simultaneously robustness and system performance of current-fed vector-controlled induction motors when parameter uncertainties are due to T_R . In [7], the mixed sensitivity problem (7) has been considered and $W_T(s)$ has been chosen as a high-pass transfer function, contradicting the experimental result presented in this paper. Therefore the solution provided in [7] bears no relationship with practice.

3.3 One-block H_∞ controller for speed control with tracking and transient performance objectives

In order to address problem P2 (angular speed control with tracking and transient performance objectives) using H_∞ control theory, the following optimisation problem must be solved

$$\text{Prob. P2: } \min_{K(s) \in S} \|W_S S\|_\infty \quad (12)$$

Writing

$$G(s) = \frac{N(s)}{M(s)} \quad (13)$$

where $N(s), M(s) \in RH_\infty$ (RH_∞ denotes the set of stable and proper transfer functions), finding $\tilde{X}(s), \tilde{Y}(s) \in RH_\infty$ that satisfy the Bezout identity

$$\tilde{X}(s)M(s) - \tilde{Y}(s)N(s) = 1 \quad (14)$$

and knowing that all stabilising controllers can be parameterised in terms of a free parameter $Q(s) \in RH_\infty$ as

$$K(s) = -\frac{\tilde{Y}(s) - M(s)Q(s)}{\tilde{X}(s) - N(s)Q(s)} \quad (15)$$

then, problem P2, can be rewritten as

$$\begin{aligned} \text{Prob. P2: } \min_{Q(s) \in RH_\infty} \|W_S(\tilde{X} - NQ)M\|_\infty \\ = \min_{Q(s) \in RH_\infty} \|\tilde{T}_1 - \tilde{T}_2 Q\|_\infty \end{aligned} \quad (16)$$

where $\tilde{T}_1(s) = W_S(s)\tilde{X}(s)M(s)$ and $\tilde{T}_2(s) = W_S(s)N(s)M(s)$. As the plant transfer function (6) is already stable, an immediate choice for $N(s), M(s) \in RH_\infty$ that satisfies (13) is given as

$$N(s) = G(s) \quad \text{and} \quad M(s) = 1 \quad (17)$$

It is therefore easy to see that the Bezout identity (14) has the following solution

$$\tilde{X}(s) = 1 \quad \text{and} \quad \tilde{Y}(s) = 0 \quad (18)$$

Consequently, the solution to optimisation problem (12) is trivial and independent of $W_S(s)$, being given by

$$Q(s) = \frac{1}{G(s)} = \frac{\tau s + 1}{k_{\text{abs}} I_{s_{\text{dref}}}} \quad (19)$$

However, this solution is improper and, therefore $Q(s) \notin RH_\infty$. In order to circumvent this problem, what is usually done [21] is to approximate this function by a rational one. This is carried out by introducing a polynomial factor $\bar{\tau}s + 1$ in the denominator of $Q(s)$, that is

$$Q_P(s) = \frac{1}{\bar{\tau}s + 1} Q(s) = \frac{\tau s + 1}{k_{\text{abs}} I_{s_{\text{dref}}} (\bar{\tau}s + 1)} \quad (20)$$

where $\bar{\tau}$ is chosen with the view to approximating $Q_P(s)$ and $Q(s)$ at the frequency range of interest. Direct substitution of $N(s), M(s), \tilde{X}(s), \tilde{Y}(s)$ and $Q_P(s)$ given by (17), (18) and (20) in the controller expression (15), followed by straightforward calculation, leads to

$$K(s) = \frac{\tau}{k_{\text{abs}} I_{s_{\text{dref}}} \bar{\tau}} \frac{\tau s + 1}{\tau s} = K_p \left(1 + \frac{1}{T_i s} \right) \quad (21)$$

where

$$K_p = \frac{\tau}{k_{\text{abs}} I_{s_{\text{dref}}} \bar{\tau}} \quad \text{and} \quad T_i = \tau \quad (22)$$

Equations (21) and (22) above show that the H_∞ controller that optimises tracking and transient performance is just the usual PI controller whose parameters are tuned according to the so-called internal model principle applied to proportional-integral-derivative (PID) controllers [22, 23]. This result explains, from the H_∞ point of view, why PI controllers have been so successfully used in vector control. However, it is worth remarking that, in order to achieve best transient performance, the tune of PI controllers must be done according to (22).

The results obtained in this section can be summarised in the following procedure.

Design procedure 1

Step 1: Set the integral time $T_i = \tau$, where τ was obtained according to experimental procedure 1.

Step 2: Choose an initial value for $\bar{\tau}$.

Step 3: Set

$$K_p = \frac{\tau}{k_{abs} I_{s,ref} \bar{\tau}}$$

Step 4: Check, through simulation, the closed-loop step response obtained for the pair (K_p, T_i) . If the transient behaviour is not satisfactory, decrease or increase $\bar{\tau}$ and go back to step 3. Otherwise, use the pair (K_p, T_i) to implement the PI controller.

3.4 Two-block H_∞ controller for speed control with tracking, transient performance and noise attenuation objectives

Speed control with tracking/transient performance and noise attenuation objectives is addressed by solving the following two-block H_∞ problem

$$\text{Prob. P3: } \min_{\text{stabilising } K(s)} \left\| \begin{bmatrix} W_S S \\ W_{KS} K S \end{bmatrix} \right\|_\infty \quad (23)$$

Using (13), (15), (17) and (18), then Problem P3 can be rewritten as

$$\text{Prob. P3: } = \min_{Q(s) \in RH_\infty} \|[T_1 - T_2 Q]\|_\infty \quad (24)$$

where

$$T_1(s) = \begin{bmatrix} W_S(s) \\ 0 \end{bmatrix}, \quad T_2(s) = \begin{bmatrix} W_S(s)G(s) \\ -W_{KS}(s) \end{bmatrix} \quad (25)$$

In order to obtain a solution to Problem P3, expressed by (24), it is first necessary to obtain an inner-outer factorisation of $T_2(s)$, as follows

$$T_2(s) = T_{2_{in}}(s)T_{2_o}(s) \quad (26)$$

where $T_{2_o}(s)$ is a stable and minimum phase transfer function and $T_{2_{in}}(s)$ satisfies the condition $T_{2_{in}}^*(s)T_{2_{in}}(s) = 1$, with $T_{2_{in}}^*(s) = T_{2_{in}}^T(-s)$. Thus, (24) can be converted to the following form

$$\text{Prob. P3: } \min_{Q(s) \in RH_\infty} \left\| \begin{bmatrix} R_1 - X \\ R_2 \end{bmatrix} \right\|_\infty \quad (27)$$

where

$$R_1(s) = T_{2_{in}}^*(s)T_1(s) \quad (28)$$

$$R_2(s) = [I - T_{2_{in}}(s)T_{2_{in}}^*(s)]T_1(s) \quad (29)$$

$$X(s) = T_{2_o}(s)Q(s) \quad (30)$$

The solution to Problem P3, expressed in terms of (27) is obtained in an iterative way [4], leading to a controller $K(s)$ that solves optimisation problem (23), as follows:

Design procedure 2

Step 1: Set $\gamma_{inf} = \|R_2\|_\infty$ and choose $\gamma > \gamma_{inf}$,

Step 2: Compute $Z_\gamma(s)$, by performing the following spectral factorisation

$$Z_\gamma(-s)Z_\gamma(s) = \gamma^2 - R_2^*(s)R_2(s)$$

Step 3: Compute $R(s) = R_1(s)/Z(s)$ and factor $R(s)$ as

$$R(s) = R_+(s) + R_-(s)$$

where $R_+(s)$ is strictly proper and anti-stable (only unstable poles), and $R_-(s)$ is stable. Let $R_+(s) = [A, b, c, 0]$ be a minimal order state-space realisation of $R_+(s)$.

Step 4: Compute W_c and W_o (the controllability and observability grammians), solutions of the following Lyapunov equations

$$AW_c + W_c A^T = -bb^T, \quad A^T W_o + W_o A = -c^T c$$

Step 5: Compute λ , the square root of the largest eigenvalue of $W_c W_o$;

Step 6: If $\lambda > 1$, choose a larger γ and go to step 2; otherwise define $\gamma_{sup} = \gamma$ and go to step 7.

Step 7: Define $\gamma = (\gamma_{inf} + \gamma_{sup})/2$ and execute, for this new value of γ , steps 2-5.

Step 8: If

(a) $\lambda > 1$, define $\gamma_{inf} = \gamma$ and go back to step 7;

(b) $\lambda < 1$, define $\gamma_{sup} = \gamma$ and go back to step 7;

(c) If $|\lambda - 1| \leq \epsilon$, where ϵ is a tolerance, go to step 9;

Step 9: Define $\tilde{R}(s) = [-A^T, c^T, b^T, 0]$ and compute a balanced realisation for $\tilde{R}(s) = [A_b, b_b, c_b, 0]$. A robust and easily implementable numerical algorithm for the computation of balanced realisations is given in [24].

Step 10: Compute the diagonal matrix Σ , solution of the following Lyapunov equations

$$A_b \Sigma + \Sigma A_b^T = -b_b b_b^T \quad \text{and} \quad A_b^T \Sigma + \Sigma A_b = -c_b^T c_b$$

Step 11: From $\Sigma = \text{diag}\{\sigma_1, \sigma_2, \dots, \sigma_n\}$, form the matrix $\Sigma_2 = \text{diag}\{\sigma_2, \dots, \sigma_n\}$ and partition A_b, b_b and c_b as follows

$$A_b = \begin{bmatrix} a_{11} & a_{12} \\ a_{21} & A_{22} \end{bmatrix}, \quad b_b = \begin{bmatrix} b_1 \\ b_2 \end{bmatrix}, \quad c_b = [c_1 \quad c_2]$$

where a_{11}, b_1 and c_1 are constants, a_{12}, a_{21}, b_2 and c_2 are vectors of dimension $n - 1$ and A_{22} is an $(n - 1) \times (n - 1)$ matrix.

Step 12: Compute

$$X(s) = [R_-(s) + X_b(s)]Z_\gamma(s)$$

where a state-space realisation for $X_b(s)$ is obtained as follows

$$\begin{aligned} \Gamma &= \Sigma_2^2 - \sigma_1^2 I_{n-1}, \quad u = -b_1/c_1 \\ \tilde{A} &= -[\Gamma^{-1}(\sigma_1^2 A_{22}^T + \Sigma_2 A_{22} \Sigma_2 - \sigma_1 u c_2^T b_2^T)]^T \\ \tilde{b} &= (c_2 \Sigma_2 + \sigma_1 u b_2^T)^T \\ \tilde{c} &= -[\Gamma^{-1}(\Sigma_2 b_2 + \sigma_1 u c_2^T)]^T \\ \tilde{d} &= -\sigma_1 u \end{aligned}$$

Step 13: Compute

$$Q(s) = T_{20}^{-1}(s)X(s)$$

Step 14: Compute

$$K(s) = \frac{Q(s)}{1 - G(s)Q(s)}$$

Step 15: Use the balanced reduction algorithm [24] to reduce the order of $K(s)$. □

It is worth remarking that all factorisations required in procedure 2 can be performed using Matlab functions.

Remark 2: An important issue in H_∞ design is the choice of weighting functions. In the case of optimisation Problem P3 (23), two weights have to be assigned by the designer: $W_{KS}(s)$ and $W_S(s)$.

Strictly speaking, tracking/transient performance of step signals cannot be considered within H_∞ control theory. This is so because steps are not ℓ_2 signals because they do not have finite ℓ_2 norm. In order to circumvent this problem, the weighting function $W_S(s)$ should be chosen so as to have a dc gain as large as possible. This makes the controller-dominant pole very close to the origin; therefore

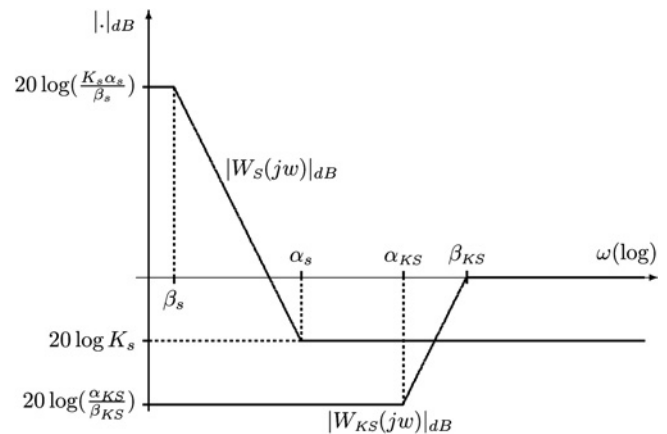


Figure 5 Asymptotes of the Bode diagrams of $W_{KS}(s)$ and $W_S(s)$

reducing, but not completely eliminating, the steady-state offset. In order to completely eliminate the resulting (small) steady-state offset, it is necessary to implement a sub-optimal H_∞ controller, obtained from the optimal by replacing the factor $(s + \beta)$, where $-\beta$ is the controller dominant pole ($\beta \simeq 0$), with s . This approximation makes the controller have a pole at the origin; therefore guaranteeing exactly tracking of step-type reference signals.

Although there is no restriction on the order of $W_{KS}(s)$ and $W_S(s)$, it is well known that the choice of high-order weighting functions leads to high-order H_∞ controllers. Therefore $W_{KS}(s)$ and $W_S(s)$ are usually chosen to be lead- and lag-transfer functions

$$W_{KS}(s) = \frac{s + \alpha_{KS}}{s + \beta_{KS}}, \quad W_S(s) = \frac{K_s(s + \alpha_s)}{s + \beta_s} \quad (31)$$

whose Bode diagrams are sketched in Fig. 5. Note in (31) that $W_{KS}(s)$ has been normalised so as to have unity gain at high frequencies. The choice of β_{KS} is dictated by the relevant noise frequency components. The gain K_s determines how smaller the penalty on $|S(j\omega)|$ (tracking and transient performance) at high frequencies should be in comparison with that on $|K(j\omega)S(j\omega)|$ (noise attenuation). Finally, assuming that β_s, K_s and β_{KS} have already been chosen, α_s and α_{KS} must be adjusted so as to establish how large the penalty on $|S(j\omega)|$ at dc-frequency should be in comparison with that on $|K(j\omega)S(j\omega)|$.

4 Experimental results

In this section, the theoretical results of the paper are validated through the implementation of H_∞ controllers in a real set-up, the induction motor whose parameters were obtained in Section 2. Although design procedures 1 and 2 lead to continuous-time H_∞ controllers, the actual implementations have been carried out in discrete time,

using the same computer and processor as those used to perform the on-off algorithm of the inverter. The equivalent discrete-time controller has been obtained using the Tustin's rule [25] with a sampling interval equal to 20 ms. In addition, there is a current limiter that constrains the reference value of the quadrature component of the stator current in the interval -15 to $+15$ A.

Consider, initially, the design of H_∞ PI-controllers to achieve tracking and best transient performance only. As $k_{abs} = 108.6936$, $\tau = 4.8703$, and, in all experiments, $I_{s, d, ref} = 2.65$ A, then, according to steps 1 and 3 of design procedure 1, the controller parameters must be tuned as

$$T_i = 4.8703 \quad \text{and} \quad K_p = \frac{\tau}{288.038\bar{\tau}}$$

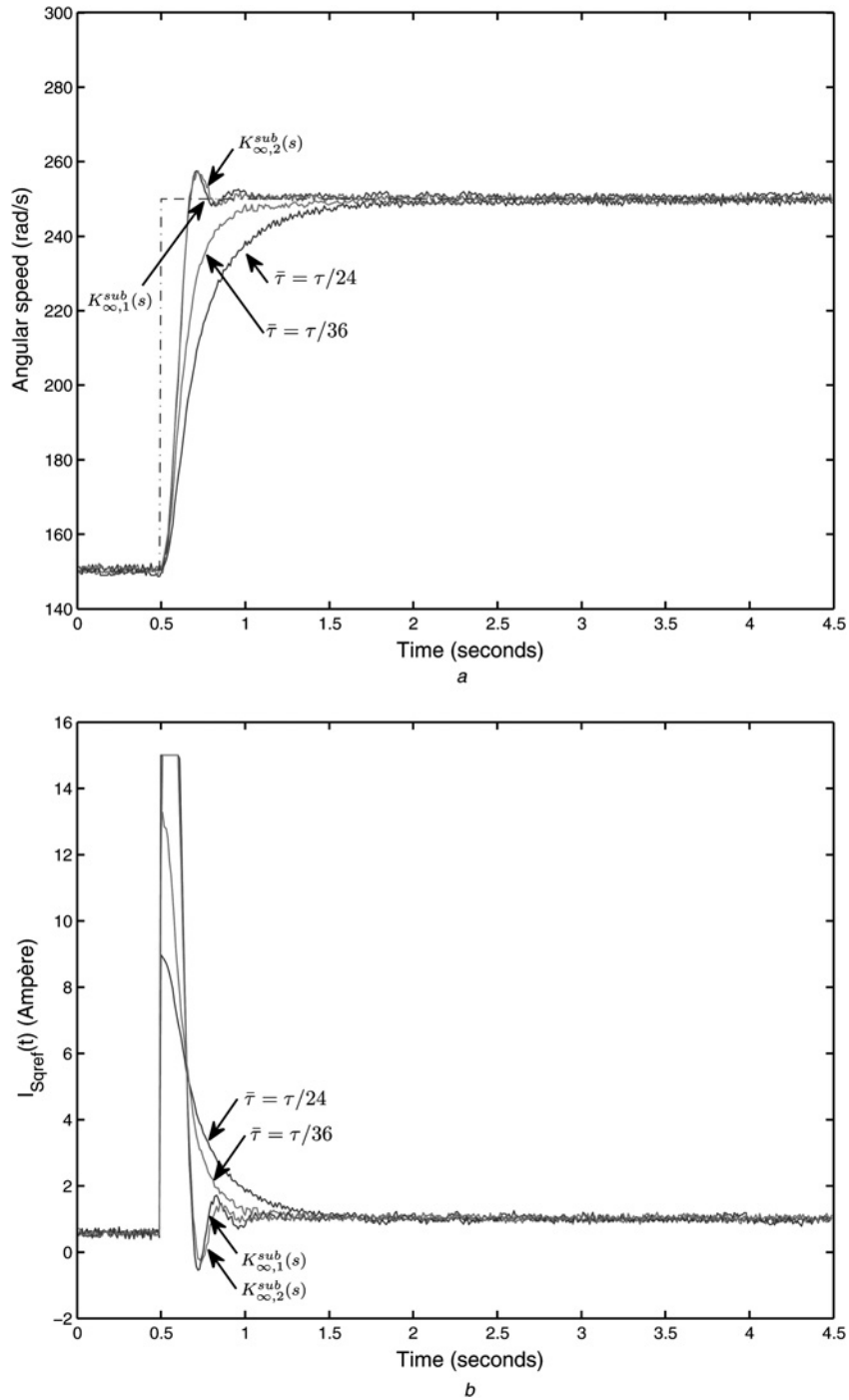


Figure 6 Closed-loop responses for

a Step reference signal of 100 rad/s of amplitude (from 150 to 250 rad/s)

b Corresponding control signal $i_{s,ref}(t)$

Obtained for H_∞ controllers for $\bar{\tau} = \tau/24$, $\tau/30$ (design procedure 1), and for $K_{\infty,1}^{sub}(s)$ and $K_{\infty,2}^{sub}(s)$ (design procedure 2)

In order to illustrate the influence of $\bar{\tau}$ in the compensated system performance, experimental results for $\bar{\tau} = \tau/24$ and $\tau/36$ are shown in Fig. 6a. The corresponding plots for the reference value of the quadrature component of stator current are shown in Fig. 6b. It can be concluded from these plots that the design strategy proposed in design procedure 1 has actually been effective to improve the closed-loop system transient performance. Indeed, a significant reduction in the system settling time has been achieved: the open-loop system settling time is approximately $t_{s_o} = 4\tau = 19.5$ s, whereas the settling times for the closed-loop systems are 1.2 and 0.85 s for $\bar{\tau} = \tau/24$ and $\tau/36$, respectively. This performance index could be reduced further but at the expense of an increase on the control signal, as one can see in Fig. 6b.

Consider now the design of two-block H_∞ controllers to achieve tracking, transient performance and noise attenuation. Two controllers have been designed to illustrate the influence of weights $W_{KS}(s)$ and $W_S(s)$. In order to obtain a compromise between tracking/transient performance degradation and noise attenuation, the following weighting functions have initially been chosen

$$W_{KS}(s) = \frac{s+30}{s+100}, \quad W_S(s) = \frac{0.2(s+15)}{s+0.01} \quad (32)$$

The resulting controller, obtained according to design procedure 2, has the following transfer function

$$K_{\infty,1}(s) = \frac{0.1548(s+100.7676)(s+0.1729)}{(s+0.01)(s+52.9590)} \quad (33)$$

As pointed out in Remark 2, since steps are not ℓ_2 signals, the two-block H_∞ controller given in (33) cannot eliminate the steady-state error and thus the step response of the closed-loop system compensated with this controller has a small steady-state error (or offset). In order to eliminate this offset, the controller to be actually implemented in practice must have a pole at the origin. This can be achieved by a controller $K_{\infty,1}^{sub}(s)$ whose transfer functions is the same as $K_{\infty,1}(s)$ except for the pole $p = -0.01$ which is replaced with $p = 0$. The closed-loop system performance and the reference value of the quadrature component of stator current for the system compensated with $K_{\infty,1}^{sub}(s)$ are shown in Figs. 6a and b, respectively. Comparing the step responses of the system compensated with $K_{\infty,1}^{sub}(s)$ and the H_∞ PI-controller with $\bar{\tau} = \tau/36$, it can be checked that although the former presents an overshoot of 7.5%, there has been a decrease in the step response settling time, which is now 240 ms.

Consider now the following choice of weights

$$W_{KS}(s) = \frac{s+30}{s+100}, \quad W_S(s) = \frac{0.1(s+15)}{s+0.01} \quad (34)$$

The resulting controller, obtained according to design procedure 2, has the following transfer function

$$K_{\infty,2}(s) = \frac{0.1105(s+101.4496)(s+0.1740)}{(s+0.01)(s+44.9685)} \quad (35)$$

As was the case for the H_∞ controller given in (33), the above controller cannot eliminate steady-state errors to step reference signals and must be replaced, in practice,

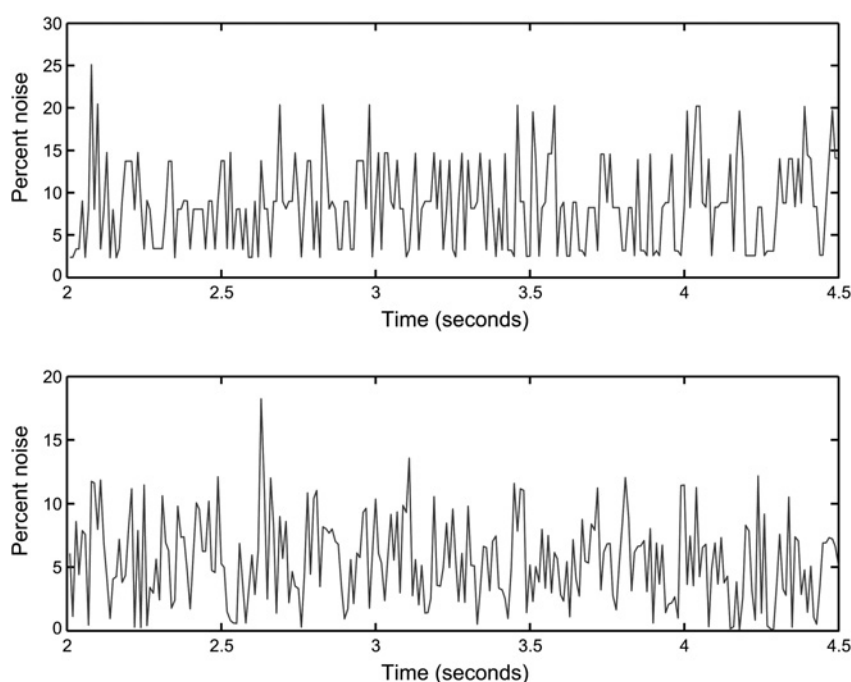


Figure 7 Per cent noise on the steady-state average value $i_{s_{ref}}$ for the H_∞ PI-controller with $\bar{\tau} = \tau/36$ (top plot), and for $K_{\infty,2}^{sub}(s)$

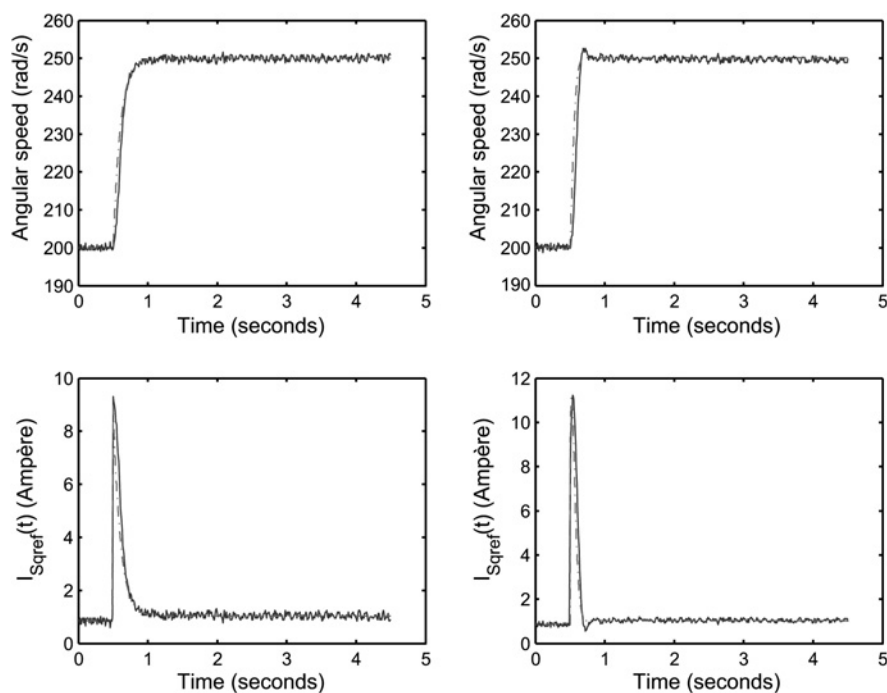


Figure 8 Comparison between real (solid lines) and simulated (dashed lines) closed-loop performance of the systems compensated with H_∞ PI-controller with $\bar{\tau} = \tau/36$ (left-side plots), and with $K_{\infty,2}^{\text{sub}}(s)$ (right-side plots)

with $K_{\infty,2}^{\text{sub}}(s)$ that is obtained from $K_{\infty,2}(s)$ by replacing the pole $p = -0.01$ with 0. The closed-loop system performance and the reference value of the quadrature component of stator current for the system compensated with $K_{\infty,2}^{\text{sub}}(s)$ are shown in Figs. 6a and b. Although the responses are quite close, it can be checked that both systems present an overshoot of 7.5% and also that there has been an increase in the settling time of the step response, which is now 260 ms. It is also important to remark that, as one can see in Fig. 6b, both two-block H_∞ controllers led $i_{s,\text{dref}}(t)$ to face a saturation in the first 0.2 s. This is due to the action of the current limiter of $i_{s,\text{dref}}(t)$ discussed at the beginning of this section. This could be avoided either by choosing different weights, although this would certainly slow down the closed-loop response, or by replacing the current supplier with a more powerful one.

As far as noise attenuation on $i_{s,\text{dref}}(t)$ is concerned, Fig. 7 presents a comparison between the per cent noise on the steady-state value of $i_{s,\text{dref}}(t)$, for the closed-loop system compensated with a H_∞ PI-controller with $\bar{\tau} = \tau/36$ (top plot) and with $K_{\infty,2}^{\text{sub}}(s)$ (bottom plot). From the plots, it can be seen that there has been a reduction on the noise amplitude: the per cent noise has been reduced, in average, from 8.6 to 5.4%. Further reduction on the noise amplitude could be achieved by choosing other weighting functions, although this would be achieved at the expenses of possible degradation in the transient performance.

An important issue addressed in this paper is the development of experiments for the estimation of the

parameters of a linear model for rotor flux-oriented current-controller induction motors. The open-loop behaviour has been verified in Section 2.3. In this section, the closed-loop behaviour of the real system is compared with the response of a Simulink model subject to same reference signal. Fig. 8 shows the closed-loop response and the reference value of the quadrature component of stator current for the systems compensated with the H_∞ PI-controller with $\bar{\tau} = \tau/36$ (left-side plots) and with $K_{\infty,2}^{\text{sub}}(s)$ (right-side plots) for the real system (solid lines) and for the Simulink model (dash-dotted lines). It can be concluded from the plots that there is a close match between simulated and real responses, attesting again the validity of the proposed model and identification scheme.

Finally, in order to submit the real induction motor drive compensated with the H_∞ PI-controller ($\bar{\tau} = \tau/36$) and with the two-block suboptimal H_∞ controller $K_{\infty,2}^{\text{sub}}(s)$ to a more challenging situation, a signal formed of positive and negative steps and also of negative and positive steps with reversion has been used as a reference signal for the angular speed. Fig. 9 shows the closed-loop system performance and the reference value of the quadrature component of stator current for the system compensated with the H_∞ PI-controller (top plots) and with $K_{\infty,2}^{\text{sub}}(s)$ (bottom plots). It can be seen from Figs. 9a and b that the closed-loop system compensated with the proposed controller has performed satisfactorily, attesting once again the efficiency of the design methodology proposed in this paper.

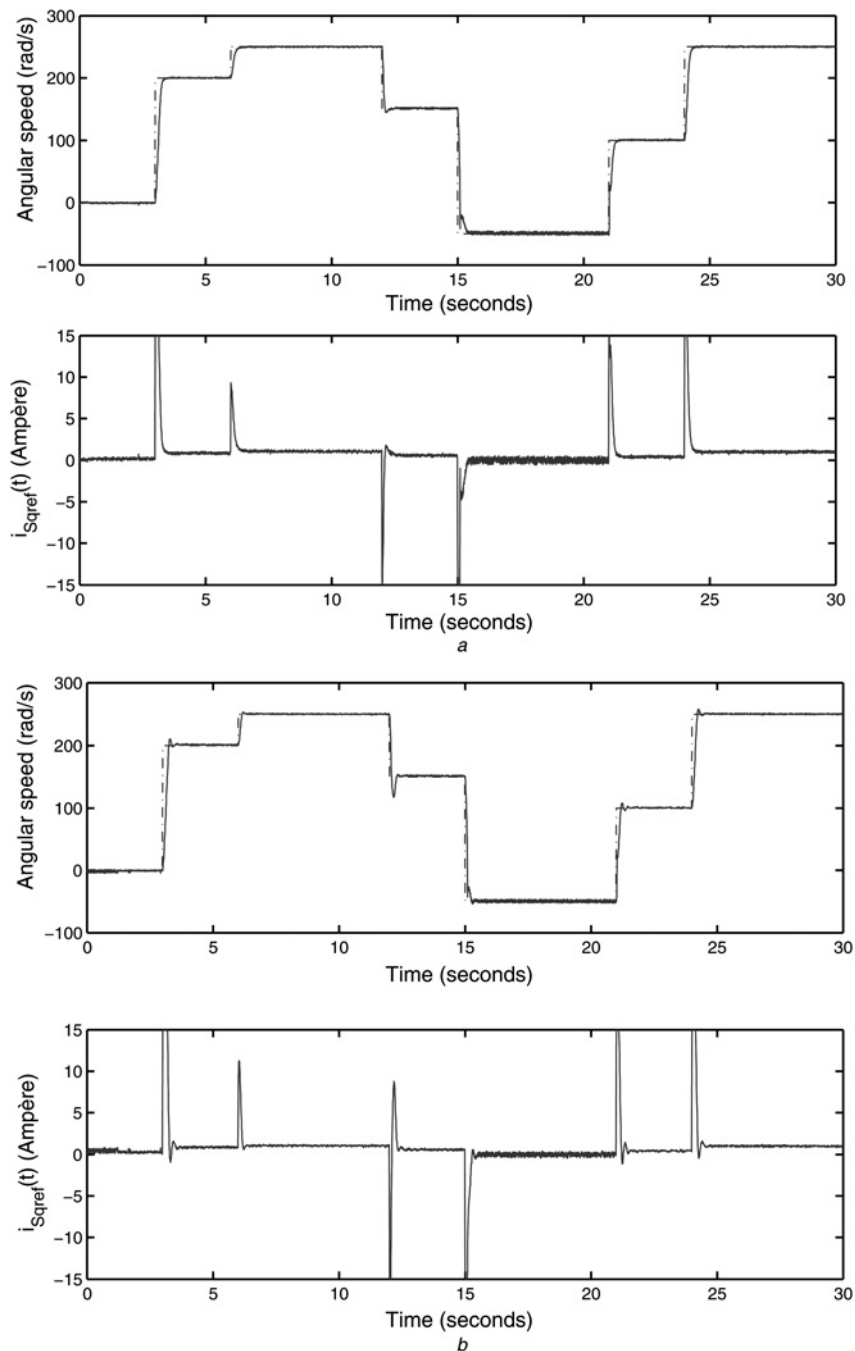


Figure 9 Closed-loop system performance of the real induction motor drive for a reference signal with positive and negative steps with changing in the rotation direction for the system controlled with an H_∞ PI-controller

a With $\bar{\tau} = \tau/36$

b With $K_{\infty,2}^{\text{sub}}(s)$

5 Conclusions

A practice-oriented design of H_∞ controllers for rotor flux-oriented current-controller induction motors is presented in the paper. All the stages of the design process are addressed. Experimental procedures for the estimation of the model parameters are presented, whose efficiency has been proved by experiments carried out in

a real set-up for both open- and closed-loop systems. As far as the actual H_∞ design is concerned, the paper has the following contributions: (i) it is presented an appropriate way to tune PI controllers to achieve best tracking/transient performance; and (ii) it has been shown how to design a controller to achieve best performance and noise reduction simultaneously; and (iii) it has been shown through experiments carried out

in a real induction motor that the mixed sensitivity problem cannot be used when the rotor time constant is the uncertain parameter.

It is also important to remark that the main purpose of the paper is to present a controller design strategy for induction motor drives that can be easily applied in practice; thus, the choice of a first-order model. Indeed, in power systems, more complex models [26] may be required because of rapid changes, such as short circuits, would excite the non-linear characteristics of the induction machine. This is an important point and might be the subject of a future research work.

6 Acknowledgment

This work was partially supported by the Brazilian Research Council CNPq, grant number 307588/2007-6.

7 References

- [1] BLASCHKE F.: 'The principle of field orientation applied to the new transvector closed-loop control system for rotating field machines', *Siemens-Rev.*, 1972, **39**, pp. 217–220
- [2] KIM D., HA I., KO M.: 'Control of induction motors via feedback linearisation with input–output decoupling', *Int. J. Control*, 1990, **51**, pp. 863–883
- [3] LEONHARD W.: 'Control of electrical drives' (Springer-Verlag, Berlin, Germany, 1996, 2nd edn.)
- [4] FRANCIS B.A.: 'A course in H_∞ control theory' (Springer-Verlag, Berlin, Germany, 1987), (LNCS, **88**)
- [5] KEEL L.H., BHATTACHARYYA S.P.: 'Robust, fragile, or optimal?', *IEEE Trans. Autom. Control*, 1997, **42**, pp. 1098–1105
- [6] MOREIRA M.V., BASILIO J.C.: 'Fragility problem revisited: overview and reformulation', *IET Control Theory Appl.*, 2007, **1**, pp. 1496–1503
- [7] KAO Y.T., LIU C.H.: 'Analysis and design of microprocessed-based vector-controlled induction motor drives', *IEEE Trans. Ind. Electron.*, 1992, **39**, pp. 46–54
- [8] ATTAIANESE C., TOMASSO G.: ' H_∞ control of induction motor drives', *IEE Proc. Electr. Power Appl.*, 2001, **148**, pp. 272–278
- [9] DOYLE J.C., GLOVER K., KHARGONEKAR P.P., FRANCIS B.A.: 'State-space solutions to standard H_2 and H_∞ control problems', *IEEE Trans. Autom. Control*, 1989, **34**, pp. 831–847
- [10] GAN W.C., QIU L.: 'Design and analysis of a plug-in robust compensator: an application to indirect-field-oriented-control induction machine drives', *IEEE Trans. Ind. Electron.*, 2003, **50**, pp. 272–282
- [11] BOTTURA C.P., NETO M.F.S., FILHO S.A.A.: 'Robust speed control of an induction motor: an H_∞ control theory approach with field orientation and μ -analysis', *IEEE Trans. Power Electron.*, 2000, **15**, pp. 908–915
- [12] DING G., WANG X., HAN Z.: ' H_∞ disturbance attenuation control of induction motor', *Int. J. Adapt. Control Signal Process.*, 2000, **14**, pp. 223–244
- [13] MAKOUF A., BENBOUZID M.E.H., DIALLO D., BOUGUECHAL N.E.: 'Induction motor robust control: an H_∞ control approach with field orientation and input–output linearising'. Proc. 27th Annual Conf. IEEE Industrial Electronics Society, Denver, USA, 2001
- [14] PREPAIN E., POSTLETHWAITE I., BENCHAI B.: 'A linear parameter variant H_∞ control design for an induction motor', *Control Eng. Pract.*, 2002, **10**, pp. 633–644
- [15] LAROCHE E., BONNASSIEUX Y., ABOU-KANDIL H., LOUIS J.P.: 'Controller design and robustness analysis for induction machine-based positioning system', *Control Eng. Pract.*, 2004, **12**, pp. 757–767
- [16] HASEGAWA M., FURUTANI S., DOKI S., OKUMA S.: 'Robust vector control of induction motors using full-order observer in consideration of core loss', *IEEE Trans. Ind. Electron.*, 2003, **50**, pp. 912–919
- [17] KAZMIERKOWSKI M.-P., MALESANI L.: 'Current control techniques for three-phase-voltage source PWM converters: a survey', *IEEE Trans. Ind. Electron.*, 1998, **45**, pp. 691–703
- [18] NAOUAR M.W., MONMASSON E., NAASSANI A.A., SLAMABELKHODJA I., PATIN N.: 'FPGA-based current controllers for ac machine drives – a review', *IEEE Trans. Ind. Electron.*, 2007, **54**, pp. 1907–1925
- [19] CHAPMAN S.J.: 'Electric machinery fundamentals' (McGraw-Hill Inc., New York, USA, 1991, 2nd edn.)
- [20] WANG K., CHIASSON J., BODSON M., TOLBERT L.M.: 'An online rotor time constant estimator for the induction machine', *IEEE Trans. Control Syst. Technol.*, 2007, **15**, pp. 330–348
- [21] DOYLE J.C., FRANCIS B.A., TANNENBAUM A.: 'Feedback control theory' (Macmillan Publishing Company, New York, 1992)
- [22] RIVERA D.E., MORARI M., SKOGESTAD S.: 'Internal model control. 4. PID controller design', *Ind. Eng. Chem. Process Des. Dev.*, 1986, **25**, pp. 252–265

[23] BASILIO J.C., MATOS S.R.: 'Design of PI and PID controllers with transient performance specification', *IEEE Trans. Educ.*, 2002, **45**, pp. 364–370

[24] GARCIA J.S., BASILIO J.C.: 'Computation of reduced-order models of multivariable systems by balanced truncation', *Int. J. Syst. Sci.*, 2002, **33**, pp. 847–854

[25] FRANKLIN G.F., POWELL J.D.: 'Digital control of dynamic systems' (Addison-Wesley, Reading, MA, 1980)

[26] KRAUSE P.C., WASYNCHUK O., SUDHOFF S.D.: 'Analysis of electrical machinery and drive systems' (IEEE Press, Piscataway, NJ, 2002, 2nd edn.)